Templating Three-Dimensional Self-Assembled Structures in Bilayer Block Copolymer Films

Vol. 24 • No. 31 • August 16 • 2012

D10488

www.advmat.de

ADVANCED MATERIALS

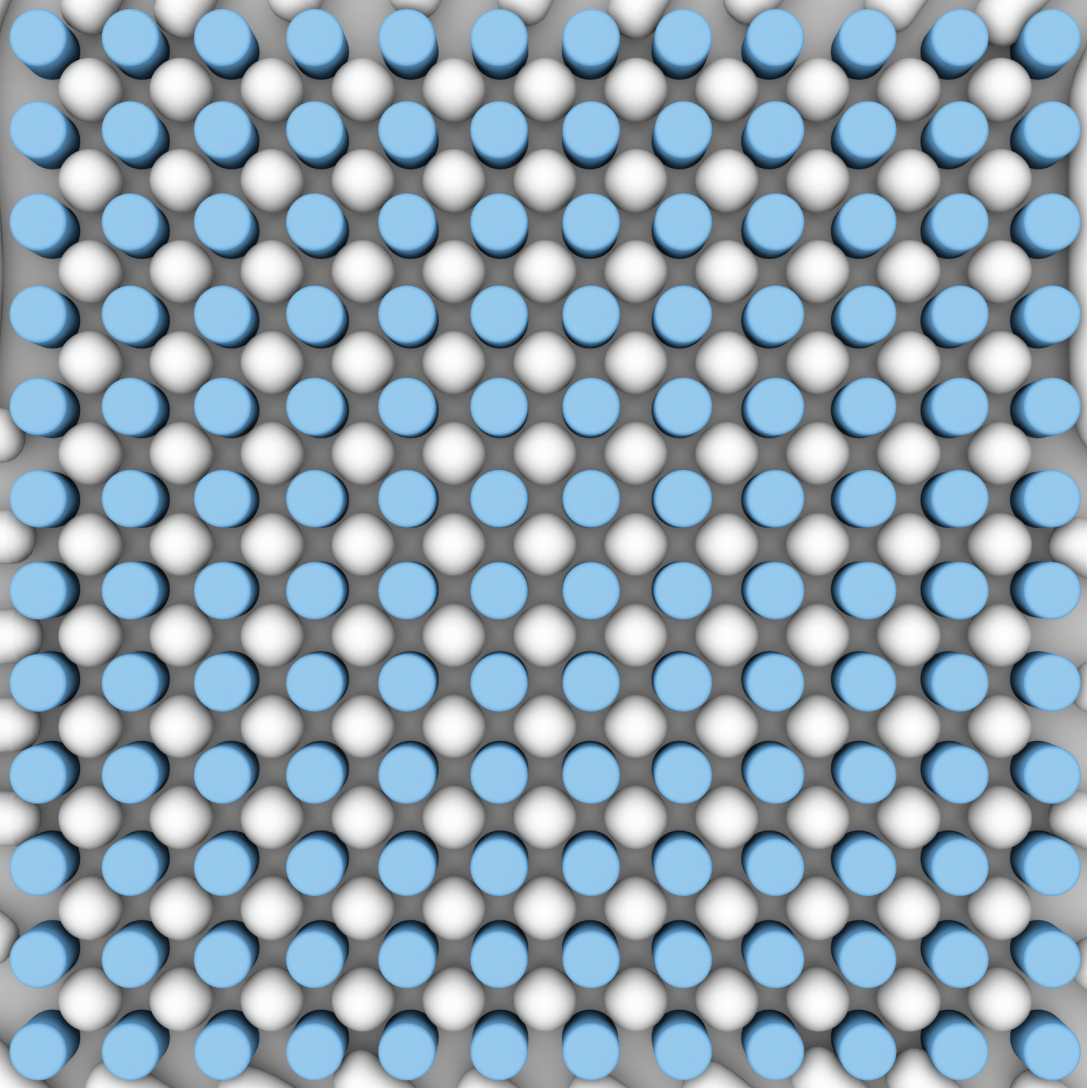

WILEY-VCH

Title: Templating Three-Dimensional Self-Assembled Structures in Bilayer Block Copolymer Films

Authors: A. Tavakkoli K. G.[1,2], K. W. Gotrik[3], A. F. Hannon[3], A. Alexander-Katz[3], C. A. Ross[3*], K. K. Berggren[1*]

Affiliations:

[1] Department of Electrical Engineering and Computer Science, Massachusetts Institute of Technology, Cambridge, MA 02139, USA.

[2] NUS Graduate School for Integrative Sciences & Engineering (NGS), Singapore 117456, Singapore.

[3] Department of Materials Science and Engineering, Massachusetts Institute of Technology, Cambridge, MA 02139, USA.

*Correspondence to: caross@mit.edu, berggren@mit.edu

Abstract: The registration and alignment of a monolayer of microdomains in a self-assembled block copolymer (BCP) thin film can be controlled by chemical or physical templating methods. Although planar patterns are useful for nanoscale device fabrication, for some applications, three-dimensional (3D) multilevel structures are required. We show that a bilayer film of a cylindrical-morphology BCP, templated by an array of posts functionalized with a brush attractive to the majority block, can form a rich variety of 3D structures consisting of cylinder arrays with controllable angles, bends, and junctions whose geometry is controlled by the template periodicity and arrangement. This technique allows control of microdomain patterns and the ability to route and connect microdomains in specific directions.

One sentence summary: We have developed a technique to control the self-assembly of cylinder-phase BCP bilayer films which allows for complex 3D geometries.

Main Text: Templated self-assembly of BCP thin films has been used for complex nanoscale pattern formation on two-dimensional (2D) surfaces by using sparse patterns of lithographically defined chemical (*1-4*) and physical templates (*5-10*). These approaches have focused on guiding a single layer of BCP microdomains which is then used as a mask to fabricate devices including patterned magnetic recording media, nanowire transistors, flash memory and gas sensors, in combination with conventional planar processing techniques such as liftoff and etching (*11-16*). However, the inherent 3D nature of self-assembled BCPs suggest their possible use in fabricating 3D devices such as cross-point structures in a single step instead of building up the structure sequentially. There have been reports of the fabrication of 3D structures by self-assembly of thicker BCP films or by sequential stacking and cross-linking of BCP films (*17-25*), but stacking methods have disadvantages for the fabrication of 3D structures due to the difficulty of aligning multiple layers, the large number of processing steps required and the poor order of the resulting patterns. In the absence of templating, the achievable geometries of bilayer BCPs are limited, for example in a bilayer cylindrical-morphology BCP thin film, the cylinders in each layer share the same orientation, while for a spherical-morphology BCP the spheres form two offset close-packed layers (*26*). Chemical templating of bilayers of spherical microdomains (*17-19*) and lamellae (*20*) has been demonstrated to form square symmetry patterns and coupled perforated lamellae respectively. A wider range of 3D BCP structures can be achieved by confinement of the BCP within parallel surfaces, narrow pores or spherical cavities, which produce structures such as helices, cylindrical shells, and stacked disks or tori not found in bulk (*24, 25, 27*). However, these processes do not enable the formation of interconnected structures in which the microdomains can be routed or connected arbitrarily over a large area.

Here we show by experiment and self-consistent field theory that simple periodic arrays of posts can give 3D control over the orientation of each layer of cylinders in a bilayer BCP film, enabling the orientation of each of the two layers of cylinders to be controlled independently, simultaneously, and locally. This was accomplished by designing the posts to be attractive to the majority block and repulsive to the minority block cylindrical microdomains by functionalizing them with a majority-block homopolymer brush. The resulting self-assembled structures are understood by considering the commensurability between the post period and the equilibrium BCP period, as well as the energy costs associated with in-phase stacking of alternate layers of cylindrical microdomains. Connections between cylinders in different layers can form a cross-point-like architecture, and by locally controlling the post periodicity and arrangement, one can design in specific defects, bends, and junctions in both top and bottom layers independently. Moreover, non-cylindrical structures such as perforated lamellae, as well as periodic superstructures with double the period of the template can be created. These results provide a strategy for making 3D structures useful in applications (e.g. cross-point memory devices) requiring the precise placement of nanowires in three dimensions. As an additional advantage, this process can produce rectangular or square-symmetric structures, which are useful in applications such as in fabricating integrated circuit interconnects or bit-patterned media (*28*).

Figure 1A shows a diagram of the major steps of the 3D templating process. In the first step, hydrogen silsequioxane (HSQ) was spin-coated at 40±2 nm thickness on Si (100) substrates. The post array templates were fabricated by means of electron-beam lithography (EBL) of the HSQ resist at 30 kV acceleration voltage, 300 pA beam current and 40 fC to 116 fC dot doses. After development and HSQ hardening by use of an oxygen plasma asher, the

final post height was 33±2 nm. Next, the substrate and posts were chemically functionalized with hydroxyl-terminated-polystyrene (1 kg mol^{-1}, 2 nm thick), which corresponds to the majority-block of the BCP. A cylindrical-morphology poly(styrene-b-dimethylsiloxane) (PS-b-PDMS) BCP (45.5 kg mol^{-1}, f_{PDMS} = 32%) was spin-coated onto the substrates with the post templates to a thickness of 42±1 nm. Solvent vapor annealing of the BCP thin film was done using a 5:1 volume ratio mixture of toluene and heptane which resulted in swelling the BCP film to 101±3 nm (~$3L_0$) and resulted in the formation of a bilayer of in-plane PDMS cylinders in a PS matrix with in-plane periodicity (L_0) of around 36 nm. Following the solvent vapor anneal, a rapid quench is done within 1 s, which was believed to freeze in the annealed morphology as the solvent vapor leaves the film (*29*). Lastly, an oxygen-reactive-ion etch (RIE) was used to remove the PS block, further reducing the film thickness and revealing the oxidized-PDMS (ox-PDMS) patterns (*30*).

Both layers of cylinders are clearly visible in scanning electron micrographs (SEMs) after etching, as shown in the examples of Fig. 1B,C, and are oriented with respect to the lattice vectors of the post lattice. The PDMS cylinders typically lie between the PS-coated posts, shown schematically in Fig. 1A (step 4), due to the PS-brush, unlike the case of PDMS-coated posts where the PDMS cylinders lie atop rows of posts (*31*). In order to describe the resulting morphologies systematically, we introduce a notation [(*a b*),(*c d*)] where (*a b*) refers to the top layer and (*c d*) refers to the bottom layer of cylinders. (*a b*) and (*c d*) are analogous to the two-dimensional Miller indexing of crystal lattice planes, i.e. if *a* = 2, then for the top layer the spacing between cylinders in the *x*-direction is half the spacing between the posts. Here the *y*-direction is that with the smaller periodicity. In cases where the cylinders lie on top of the posts, an apostrophe e.g. (*a b*)' was included in the notation. Some post lattices generate non-

cylinder morphologies, which are designated “S”, “E” or “B” for spheres, ellipsoids, or bicontinuous cylinders (perforated lamellae), respectively, in place of the Miller indices.

Figure 1B shows a bilayer film templated by a rectangular array of PS-functionalized posts with 21 nm diameter, 33 nm height, and 36 nm and 100 nm periods in the *x*- and *y*-directions, respectively. Fig. 1C shows magnified and cross-sectional SEMs of regions inside and outside the templated region. Outside the templated region, the top and bottom layers of ox-PDMS cylinders shared local orientation, with the cylinders in the top layer lying in between those of the bottom layer without showing long-range order. Inside the templated region, the cylinders in the top and bottom layers did not generally share local orientation between the posts due to the energetic cost associated with incommensurability. As a result, the top cylinders instead self-assembled into a mesh-like array that covered the entire templated region (see fig. S1 for an example where the cylinders form a different angle between the two layers and fig. S2 for a cross-sectional image from a different viewing angle). Fig. 1D,E shows another example of templated bilayer films in which additional columns of square or parallelogram-shaped holes were generated between the posts. These results demonstrate the ability to control the orientation of the individual layers of microdomains within a bilayer, and make use of majority-block brush-coated posts, which is unlike our earlier work on single-layers of microdomains templated by minority-block brush-coated posts (31).

By changing the post periodicities in the *x*- and *y*-directions, we achieved a wide range of orientations and morphologies of both the top and bottom layers of microdomains. Figure 2 shows examples including parallel top and bottom PDMS cylinders (Fig. 2A-B), mesh-like structures (Fig. 2C-F), structures containing a layer of ellipsoids, spheres, or bicontinuous cylinders (E, S, and B in Fig. 2G-I), and periodic superstructures (Fig. 2J-K). Each of these 3D

structures was observed within specific ranges of post periodicities in the *x*- and *y*-directions, and the cylinders were oriented perpendicular to the direction in which the post periodicity was commensurate with the BCP period. In general the top layer of cylinders formed the more commensurate arrangement. These structures are consistent with the mesh-shaped equilibrium morphologies observed in the self-consistent field theory (SCFT) simulations which modeled the morphologies present when the film was fully swollen, before quenching.

Figure 2A,B shows cases where the cylinders in both layers were oriented parallel (in the *y*-direction, Fig. 2A and in the diagonal direction, Fig. 2B) and the cylinders in the top layer were offset from those of the bottom layer, as seen in the untemplated bilayer film. The offset stabilizes the parallel arrangement, but it incurs an energy penalty if there is contact between the cylinders and posts. The top layer of cylinders could overlay the posts (Fig. 2B), but in cases where the bottom layer lay along a line of posts it was interrupted to form dash shapes (fig. S3).

In Fig. 2C-F, the cylinders in the two layers oriented in two different directions and made a mesh-shaped structure. Mesh-shaped structures occurred when the post period in the *y*- or diagonal direction was equal to the BCP period, favoring alignment of one layer of cylinders perpendicular to the *y*- or diagonal direction, but the period in the *x*-direction was slightly less than an integer-multiple of the BCP period. In this case the parallel alignment seen in Fig. 2A,B is less favorable than a mesh structure. Depending on the commensurability of the post lattice, the angle of the mesh was 90˚ (Fig. 2C,E) or more (Fig. 2D,F).

The mesh structures of Fig. 2C-F can be generalized to include larger numbers of cylinders subdividing the x-axis period, as shown in Fig. 1D,E, where the post periods in the *x*-direction were less than four times the BCP period. The dimensions of the square and

parallelogram holes in all the mesh-shaped patterns were 18×18 nm^2 and their periods in the *y*- and diagonal directions were about 36 nm, matching the BCP period. The resulting parallelogram and square holes demonstrated sharp corners relative to those fabricated using conventional lithography, suggesting a role for such structures in the generation of nanoscale square or rhombic features or pits.

Fig. 2G-I shows examples in which the bottom layer of microdomains formed ellipsoids (Fig. 2G) and spheres (Fig. 2H) in between the posts, and bicontinuous cylinders or perforated lamellae (Fig. 2I) in which the holes in the PDMS surrounded the posts. These structures occurred when the BCP period was not commensurate with either the *x* or the *y*-direction spacing. We also observed periodic superstructures in which the structure alternated between two morphologies between adjacent rows of posts, resulting in twice the period of the post lattice. Examples are given in Fig. 2J,K.

To analyze the experimental morphologies, we constructed in Fig. 2L a phase diagram where the various morphologies are plotted as a function of post period P_x and P_y in the *x*- and *y*-directions, respectively. The periods are expressed as multiples of L_0, the equilibrium period of cylinders in an untemplated film annealed under the same conditions. Post arrays in which no dominant structure, or poorly ordered structures, occurred are represented with small black dots while ordered structures are shown with larger symbols. Superposed on this graph are vertical and horizontal colored bands representing approximate commensurate conditions, i.e. when P_x and P_y are within ± 9% of an integer multiple of L_0. Curved colored bands represent commensurate conditions for the diagonal spacing, e.g. $(P_x^2 + P_y^2)^{0.5}$. A value of 9% was chosen because BCP films have been found to adjust their period in response to a template by up to approximately this amount (*31, 32*).

Examination of Fig. 2L shows that the observed morphologies correspond well with the commensurate template conditions. For example, blue circles, representing cylinders oriented along the *y*-direction, appear within the vertical colored band; red circles within the horizontal colored band, and red and blue triangles (representing diagonally-oriented cylinders) within the curved band. Green circles and triangles correspond to the perpendicular and angled mesh-shaped structures. The values of P_x and P_y outside the bands produce poorly ordered or mixed structures, or bicontinuous cylinder structures in a few cases. The correspondence indicates that commensurability in both *x* and *y*-directions plays a dominant role in determining which morphology forms.

SCFT simulations were carried out to investigate both the 3D structure of the features as well as the metastability of the structures observed (see supplementary online text). The thickness of the unit cell was set to the swelled BCP thickness observed during the solvent annealing, which was ~3.00 L_0, and the post diameter and height were 0.71 L_0 and 1.64 L_0, respectively (see supplementary online text). The simulation showed the same general trends as the experiments. Parallel cylinders were predicted by the SCFT simulation for *x*-direction post periods equal to integer multiples of L_0 (Fig. 2M). Perpendicular mesh-shaped structures were predicted for *x*-direction periods less than an integer multiple of L_0 ($2L_0$, $3L_0$) and *y*-direction periods equal to L_0, as was seen in the experiments (Fig. 2N,O). Different morphologies in the two layers were predicted by SCFT such as cylinders over spheres (Fig. 2P) and cylinders over bicontinuous cylinders (Fig. 2Q). However, simulations of two unit cells did not predict the observed superstructures. To explain these structures, factors not included in the SCFT such as bending of the posts or non-equilibrium formation during the

solvent vapor annealing may be important. Recently, crossed cylinders were also predicted in a BCP confined between parallel surfaces with highly incommensurate spacing (*27*).

In the simulations, the cylinders in the two layers were often connected, as shown in Fig. 2N-P. These connections between the two layers may be metastable defects. However, there is also experimental evidence in the mesh shaped-structures for these connections (fig. S9). By seeding the simulation with a field configuration that represented a mesh shaped-structure without a connection, we found that the energies of the connected vs. unconnected systems were too close to distinguish a lower energy state (see supplementary online text). Thus, local connections between cylinders are likely to be present in the system and should be considered in post-processing applications for these patterns.

We have so far shown that control of the alignment and the morphology of the PDMS microdomains in two different layers. We were also able to locally control the post periodicity and arrangement to form more complicated patterns with specific defects, bends and neighboring junctions. In particular, junctions and bends were placed in either of the layers of cylindrical microdomains. Two strategies or a combination of them were used to fabricate such aperiodic structures: (1) a rectangular post array with a variation in the post periodicity in one or both directions to fabricate bends and junctions (T- and angled-junctions) in the top layer; and (2) a post lattice whose orientation varied while the period was constant to fabricate bends and junctions (T-, angled- and Y-junctions) in the bottom layer. These types of bends and junctions could potentially be used to fabricate integrated-circuit elements (*33*). Fig. 3A shows a structure made by the first strategy in which, by increasing the post periodicity in the *x*-direction, a [(0 1),(2 0)] structure joined with a [(3 0),(2 0)] structure and, by increasing the post periodicity in the *y*-direction and decreasing it in the *x*-direction, the [(3 0),(2 0)] structure

joined with a [(1 1),(2 0)] structure. Thus the bottom layer of cylinders had a fixed direction (*y*-direction) and only the direction of the top cylinders was varied; structures such as T-junctions formed where the different orientations meet. Fig. 3B shows a structure made using the second strategy in which, by changing the post arrangement, the [(-1 1),(2 0)] structure contained a mirror-plane. The top layer of cylinders had a fixed direction (*x*-direction) and only the direction of the bottom cylinders was varied. Fig. S14 shows an example of a Y-junction in which two cylinders merged into one cylinder, and Figs S15-S17 show additional images of similarly fabricated structures.

The central result of this work is the independent and simultaneous control of the morphology and orientation of two layers of BCP microdomains and the demonstration and explanation of the factors that govern the 3D arrangement of cylindrical microdomains in response to an array of posts functionalized with a majority block brush. A wide range of morphologies was observed as a function of post period, and analyzed in terms of the relation between the post period and equilibrium period of the BCP. By locally altering the post period and orientation, more complicated structures such as specific defects, bends and junctions were achieved, and connections between the top and bottom layers of cylinders were demonstrated (fig. S18). Non-cylindrical morphologies such as spheres, ellipsoids or bicontinuous cylinders as well as superstructures were also created at certain post periods. As an additional advantage, this method enables formation of square and rectangular symmetry meshes. This work provides strategies for the 3D routing of dense nanoscale cylindrical features on substrates using a single self-assembly step, which could facilitate new methods for nanoscale device manufacturing.

References and Notes

1. R. Ruiz *et al.*, Density multiplication and improved lithography by directed block copolymer assembly. *Science* **321,** 936-939 (2008).
2. J. Y. Cheng, C. T. Rettner, D. P. Sanders, H. Kim, W. D. Hinsberg, Dense self-assembly on sparse chemical patterns: Rectifying and multiplying lithographic patterns using block copolymers. *Adv. Mater.* **20,** 3155-3158 (2008).
3. S. O. Kim *et al.*, Epitaxial self-assembly of block copolymers on lithographically defined nanopatterned substrates. *Nature* **424,** 411-414 (2003).
4. L. Rockford, Y. Liu, P. Mansky, T. P. Russell, Polymers on nanoperiodic, heterogeneous surfaces. *Phys. Rev. Lett.* **82,** 2602-2605 (1999).
5. I. Bita *et al*., Graphoepitaxy of self-assembled block copolymers on two-dimensional periodic patterned templates. *Science* **321,** 939-943 (2008).
6. S. Park *et al.*, Macroscopic 10-terabit-per-square-inch arrays from block copolymers with lateral order. *Science* **323,** 1030-1033 (2009).
7. R. A. Segalman, H. Yokoyama, E. J. Kramer, Graphoepitaxy of spherical domain block copolymer films. *Adv. Mater.* **13,** 1152-1155 (2001).
8. J. Y. Cheng, C. Ross, E. L. Thomas, H. I. Smith, G. J. Vancso, Templated self-assembly of block copolymers: Effect of substrate topography. *Adv. Mater.* **15,** 1599-1602 (2003).
9. C. T. Black, O. Bezencenet, Nanometer-scale pattern registration and alignment by directed diblock copolymer self-assembly. *Nanotechnology, IEEE Trans. on* **3,** 412-415 (2004).
10. R. Ruiz, R. L. Sandstrom, C. T. Black, Induced orientational order in symmetric diblock copolymer thin films. *Adv. Mater.* **19,** 587– 591 (2007).

11. D. J. Milliron, S. Raoux, R. Shelby, J. Jordan-Sweet, Solution-phase deposition and nanopatterning of GeSbSe phase-change materials. *Nature Mater.* **6,** 352–356 (2007).

12. J. Y. Cheng, W. Jung, C. A. Ross, Magnetic nanostructures from block copolymer lithography: hysteresis, thermal stability and magnetoresistance. *Phys. Rev. B* **70,** 064417 (2004).

13. C. T. Black, Self-aligned self assembly of multi-nanowire silicon field effect transistors. *Appl. Phys. Lett.* **87,** 163116 (2005).

14. T. Thurn-Albrecht *et al.*, Ultrahigh-density nanowire arrays grown in self-assembled diblock copolymer templates. *Science* **290,** 2126–2129 (2000).

15. K. Naito, H. Hieda, M. Sakurai, Y. Kamata, K. Asakawa, 2.5-inch disk patterned media prepared by an artificially assisted self-assembling method. *IEEE Trans. Magn.* **38,** 1949–1951 (2002).

16. Y. S. Jung, W. Jung, H. L. Tuller, C. A. Ross, Nanowire conductive polymer gas sensor patterned using self-assembled block copolymer lithography. *NanoLett.* **8,** 3776–3780 (2008).

17. S. Ji *et al*., Three-dimensional directed assembly of block copolymers together with two-dimensional square and rectangular nanolithography*, Adv. Mater.* **23**, 3692–3697 (2011).

18. S.-M. Park, G. S. W. Craig, Y.-H. La, P. F. Nealey, Morphological reconstruction and ordering in films of sphere-forming block copolymers on striped chemically patterned surfaces**,** *Macromolecules* **41**, 9124-9129 (2008).

19. S. M. Park, G. S. W. Craig, Y.-H. La, H. H. Solak, P. F. Nealey, Square arrays of vertical cylinders of PS-b-PMMA on chemically nanopatterned surfaces. *Macromolecules* **40**, 5084-5094 (2007).
20. K. Ch. Daoulas *et al*., Fabrication of Complex Three-Dimensional Nanostructures from Self-Assembling Block Copolymer Materials on Two-Dimensional Chemically Patterned Templates with Mismatched Symmetry. *Phys. Rev. Lett.* **96**, 036104 (2006).
21. H. Jung *et al*., Three-Dimensional multilayered nanostructures with controlled orientation of microdomains from cross-linkable block copolymers. *ACS Nano* **5,** 6164-6173 (2011).
22. F. Rose, J. K. Bosworth, E. A. Dobisz, R. Ruiz, Three-dimensional mesoporous structures fabricated by independent stacking of self-assembled films on suspended membranes. *Nanotechnology* **22,** 035603 (2011).
23. E. Kim *et al*., Size control and registration of nano-structured thin films by cross-linkable units. *Soft Matter* **4,** 475-479 (2008).
24. Y. Wu *et al*., Composite mesostructures by nano-confinement. *Nature Mater.* **3,** 816-822 (2004).
25. K. Shin *et al*., Curving and frustrating flatland. *Science* **306,** 76 (2004).
26. C. S. Henkee, E. L. Thomas, L. J. Fetters, The effect of surface constraints on the ordering of block copolymer domains. *J. Mater. Sci.* **23,** 1685-1694 (1988).
27. B. Yu, B. Li, Q. Jin, D. Ding, A. C. Shi, Confined self-assembly of cylinder-forming diblock copolymers: effects of confining geometries. *Soft Matter* **7,** 10227-10240 (2011).

28. R. Ruiz, E. Dobisz, T. R. Albrecht, Rectangular patterns using block copolymer directed assembly for high bit aspect ratio patterned media. *ACS Nano* **5**, 79–84 (2011).
29. W. A. Phillip, M. A. Hillmyer, E. L. Cussler, Cylinder orientation mechanism in block copolymer thin films upon solvent evaporation**,** *Macromolecules* **43**, 7763-7770 (2010).
30. Materials and methods are available as supplementary material on Science Online.
31. J. K. W. Yang *et al.*, Complex self-assembled patterns using sparse commensurate templates with locally varying motifs. *Nature Nanotech.* **5,** 256-260 *(2010).*
32. M. P. Stoykovich *et al*., Directed assembly of block copolymer blends into nonregular device-oriented structures. *Science* **308,** 1442 (2005).
33. M. P. Stoykovich *et al*., Directed self-assembley of block copolymers for nanolithography: fabrication of isolated features and essential integrated. *ACS Nano* **1**, 168-175 (2007).
34. J. K. W. Yang, K. K. Berggren, Using high-contrast salty development of hydrogen silsesquioxane for sub-10-nm half-pitch lithography. *J. Vac. Sci. Technol.* **25,** 2025 (2007).
35. C. A. Ross *et al*. Si-containing block copolymers for self-assembled nanolithography. *J. Vac. Sci. Technol.* **26,** 2489 (2008).
36. S. J. Ashcroft, A.D. Clayton, R. B. Shearn, Isothermal vapor-liquid equilibriums for the systems toluene-n-heptane, toluene-propan-2-ol, toluene-sulfolane, and propan-2-ol-sulfolane, *J. Chem. Eng. Data* **24**, 195-199 (1979).
37. R. A. Mickiewicz *et al*., Enhancing the potential of block copolymer lithography with polymer self-consistent field theory simulations. *Macromolecules* **43,** 8290-8295 (2010).

Acknowledgements: The authors acknowledge support from the Semiconductor Research Corporation, the FENA Center, NRI, SMA, National Science Foundation, Tokyo Electron and Taiwan Semiconductor Manufacturing Company. A.T.K.G would like to express his profound gratitude to Professor T. C. Chong and Dr. S. N. Piramanayagam for their support, and would like to acknowledge his fellowship from NGS Singapore. The Research Laboratory of Electronics Scanning-Electron-Beam Lithography Facility provided facilities for this work. The authors also thank M. Mondol and J. Daley for technical assistance. A Patent titled "Removable Templates for Directed Self-assembly" has been filed with MIT.

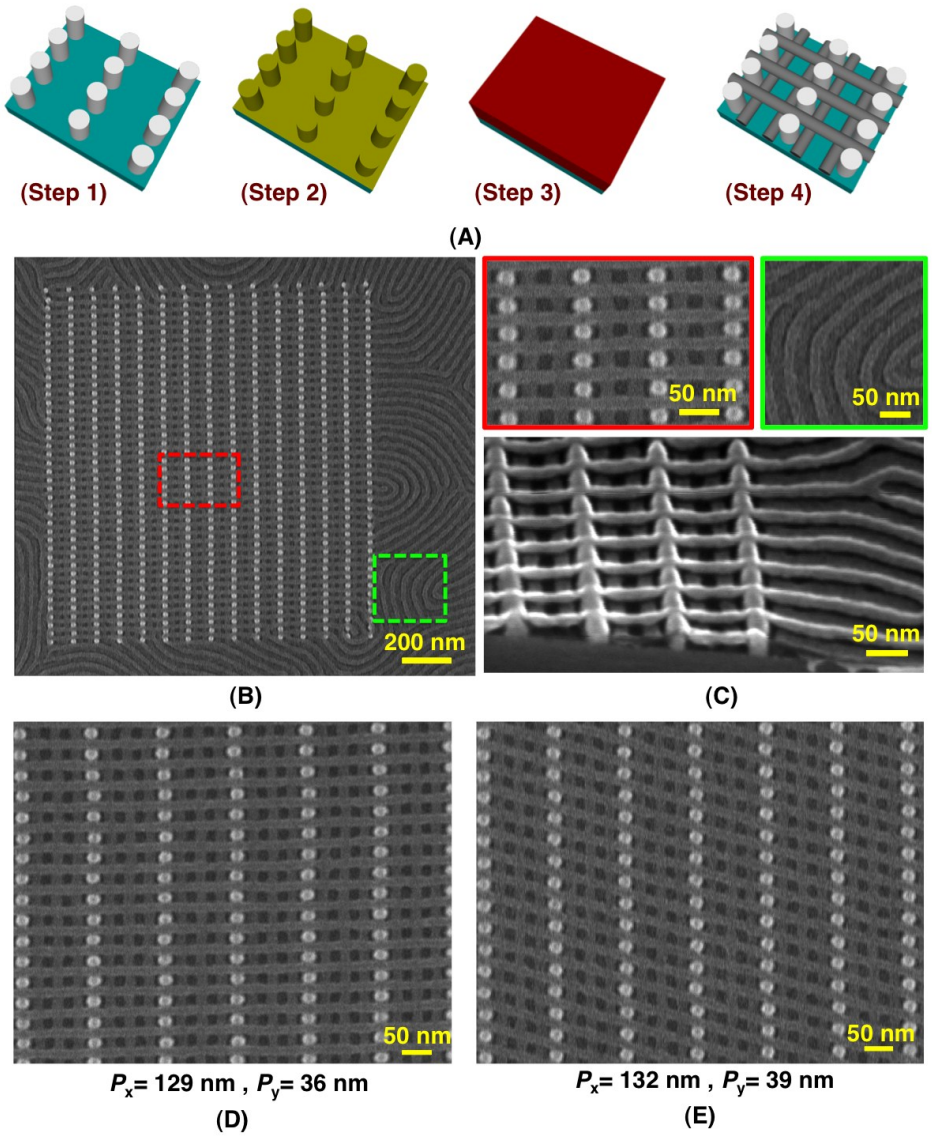

Figure 1. Fabrication of 3D structures. **(A)** The major steps of the fabrication process for the 3D structures: (step 1) fabricating the post templates by EBL, (step 2) chemically functionalizing posts with a PS brush, (step 3) spin-coating and solvent-annealing of the BCP, (step 4) removing the PS matrix by an oxygen RIE and leaving the ox-PDMS patterns on the substrate. (**B**) SEM of an etched [(0 1),(2 0)] bilayer structure on a substrate. (**C**) Magnified and cross-sectional SEMs of the regions inside and outside the post-templated region. (**D**) and (**E**) SEMs of a [(0 1),(3 0)] perpendicular and a [(1 1),(3 0)] angled mesh-shaped structures formed from two layers of ox-PDMS cylinder arrays, respectively. The bright dots and the light grey linear features represent HSQ and ox-PDMS, respectively.

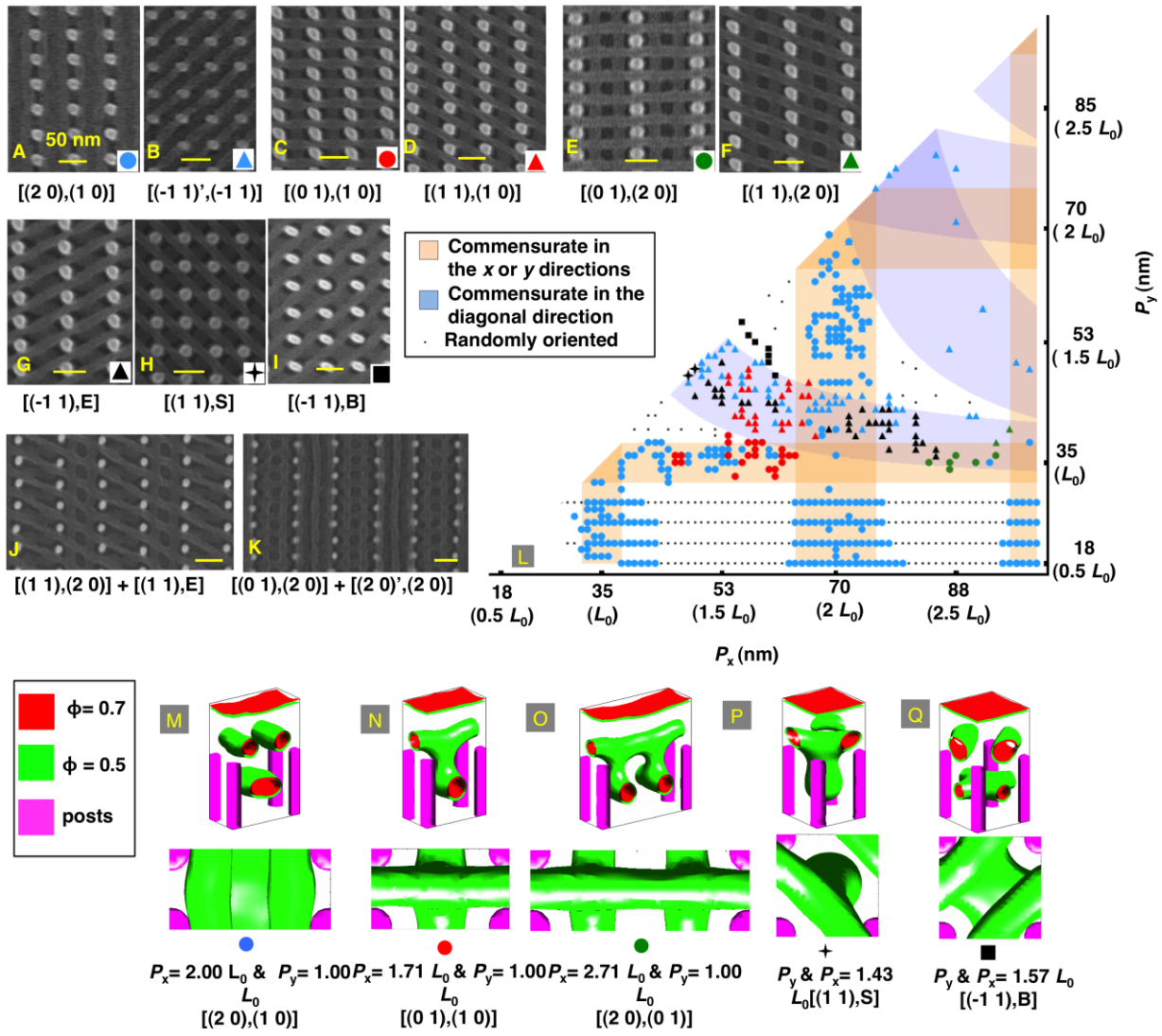

Figure 2. Templating and modelling 3D self-assembled structures. (**A-K**) SEMs of the ox-PDMS microdomains templated by post arrays. White and light gray shades represent HSQ posts and ox-PDMS, respectively. Ox-PDMS microdomains, (**A-B**) were commensurate in the same direction; (**C-F**) formed perpendicular and angled mesh-shaped structures; (**G-I**) formed two different morphologies on top of each other (cylinders on top of (**G**) ellipsoids; (**H**) spheres; (**I**) bicontinuous cylinders); (**J-K**) formed periodic superstructures. (see figs. S3-S8, for larger and colorized images). (**L**) A map showing a summary of the experimentally determined morphologies. Circle shapes refer to cylinders along *x* or *y*. Triangle, star and square shapes refer to cylinders oriented in a diagonal direction. (**M-Q**) SCFT simulation results for representative post periods. Top images are isometric views and bottom images are top-down views. Surface contours of constant minority block (PDMS) density ϕ are plotted with ϕ = 0.5 representing the boundary between the PS and PDMS blocks.

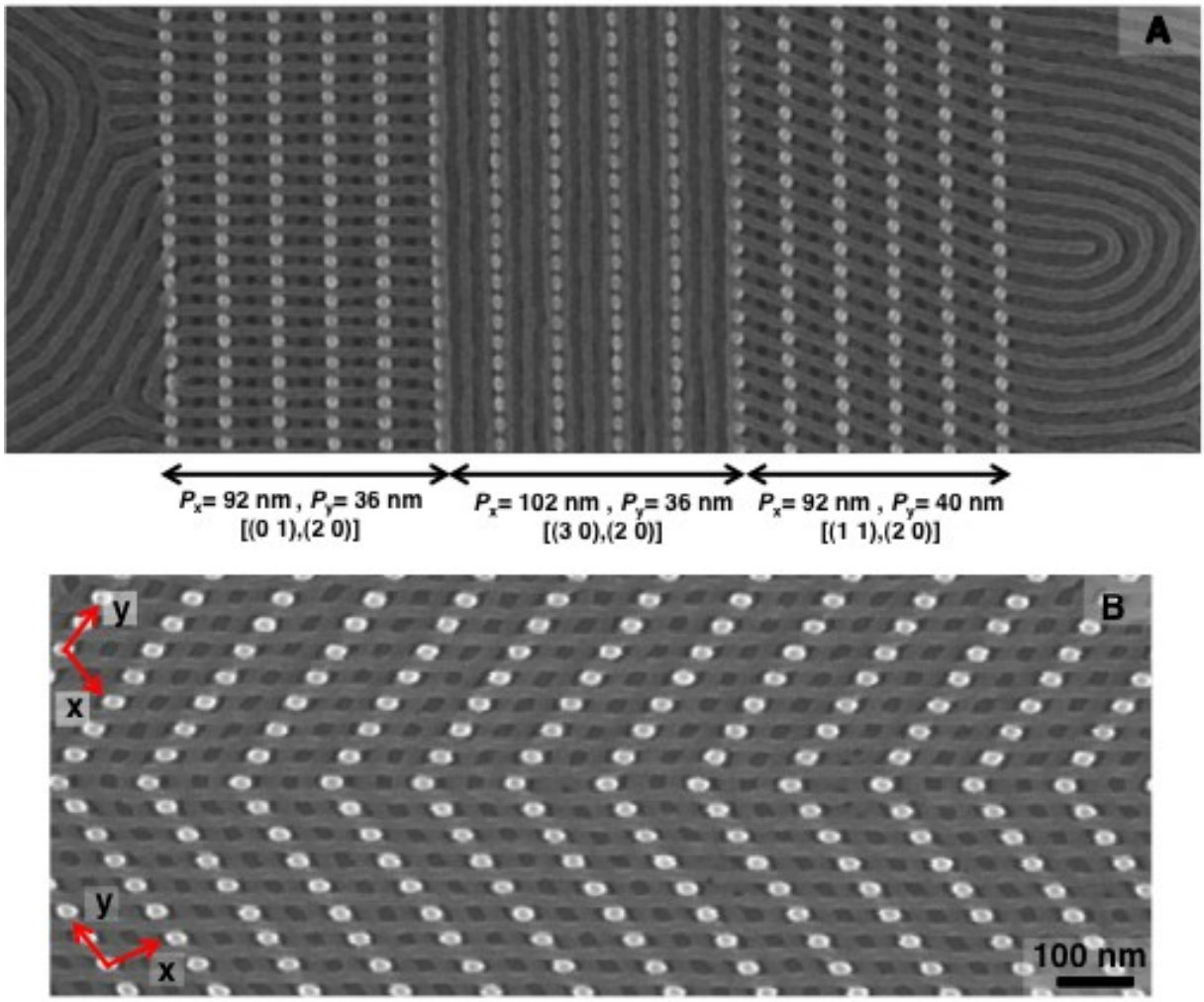

Figure 3. Templated 3D bends and junctions. (**A)** SEM of a locally controlled structure fabricated by changing the post periodicity in the *x*- and *y*-directions. Left to right, the structures changed from [(0 1),(2 0)] to [(3 0),(2 0)] and then to [(1 1),(2 0)]. **(B)** SEM of a locally controlled structure fabricated by changing the post lattice orientation. Top to bottom, the [(-1 1),(2 0)] structure contained a mirror plane. The *x* and *y* axes make an angle of 107˚. White and light grey contrast represent HSQ and ox-PDMS, respectively.

Supporting Online Material

Materials and Methods

Figs. S1 to S16

References (*34-37*)